Computational and Theoretical Chemistry 1231 (2024) 114403

Contents lists available at ScienceDirect

Computational and Theoretical Chemistry

journal homepage: www.elsevier.com/locate/comptc

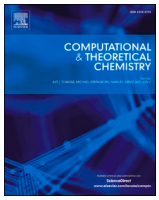

Metal-adorned borophene for efficient glucose adsorption

Marisol Ibarra-Rodríguez [a,*], Paul Horley [b], Mario Sánchez [b,*]

[a] Universidad Autónoma de Nuevo León, Facultad de Ciencias Químicas, Ciudad Universitaria, 66455 San Nicolás, Nuevo León, México
[b] Centro de Investigación en Materiales Avanzados, S.C., Alianza Norte 202, PIIT, Carretera Monterrey-Aeropuerto Km. 10, C. P. 66628 Apodaca, Nuevo León, México

ARTICLE INFO

Keywords:
Borophene
DFT
Drug delivery
Glucose

ABSTRACT

In view of the urgent need for developing new materials for biomedical applications, we report on multi-facet study of functionalized borophene as a possible sensor or transporter of glucose. The adsorption of a glucose molecule on $[MB_{36}]^{+}$(M = Li, Na, K), $[MB_{36}]^{2+}$ (M = Be, Mg, Ca), and $[MB_{36}]^{3+}$ (M = B, Al, Ga) complexes were studied both in gas and in water phase, conforming that $[MB_{36}]^{+}$, $[MB_{36}]^{2+}$, $[MB_{36}]^{3+}$ are highly efficient as glucose adsorbers with the binding energies of −34 to −135 kcal/mol in the gas phase, and −12 to −111 kcal/mol in water as calculated with the PBE0-D3/def2-TZVP. Borophene adorned with beryllium have the highest adsorption energies, while the complexes with Li, Na and K are characterized with lower binding energy values. Thus, the systems with 1+ oxidation state are more promising for intelligent drug delivery, while $[MB_{36}]^{+}$, $[MB_{36}]^{2+}$, $[MB_{36}]^{3+}$ are more suitable for designing biosensors of glucose.

1. Introduction

The new two-dimensional material called borophene attracted much attention in the scientific circles. Borophene is a mono-element compound with large specific surface area. It behaves as anisotropic metal and features remarkable mechanical properties.[1–4] Several different allotropes of borophene exist. Among these, the borophene B_{36} is a stable quasi-planar compound with hexagonal symmetry.[5,6] Chemical and physical properties of borophene make it attractive for different types of applications, including energy storage,[7,8] electronics,[9] and biomedicine. [10–14] A fragment of borophene features a small central cavity, which can be useful for coordination with other atoms or molecules. For example, the addition of metals modifies the structure of borophene, improving material stability and permitting careful tailoring of its physical and chemical properties.

B_{36} is very promising for biomedical applications, including the timely and important tasks such as intelligent drug delivery. The surface area of borophene provides sufficient space for drug loading and enough anchor points for functional groups, which are the principal requirements for materials used in anti-cancer drug delivery; several research groups actively work in this direction.[10,15,16] Recently, an *in vivo* study of 2D borophene nanoflakes loaded with hemocytes of the beetle *T. molitor* revealed that no hemocytotoxicity was induced in short-term experiments for the doses of 0.5, 1 or 2 μg nanoflakes per insect. [17] In humans, the toxicological profile of borophene was studied using the cell viability analysis.[18] The viability of human macrophage cells was 84.2% and 88.5% after treatment with 100 μg/mL borophene nanosheets and borophene nanosheets − corona complexes. Importantly, proteomics studies revealed that 46.5% of the proteins bound to borophene nanosheets (94 plasma proteins) are immune-relevant proteins.

Borophene is also promising as a biosensor of gases: its large surface area offers considerable adsorption capacity of gas molecules. Borophene has been studied as a possible sensor for ethanol[19] and ammonia.[20] This material has been also used for the adsorption of highly toxic gases such as formaldehyde, CO, and NO.[20,21].

Another high-priority biomedical application concerns the monitoring of blood glucose levels for diabetes control. A number of research teams developed different types of materials with acute glucose sensing abilities. Jadoon *et al.*[22] reported silver-graphene quantum dots as promising for glucose detection. They found that silver-coated coronene has better sensing ability in comparison to that of H_2O_2. Caglar and colleagues [19] studied theoretically the addition of Pd to *N*-doped graphene surface, promoting glucose electro-oxidation in alkaline media and its adsorption by Pd-G and Pd-3N graphene. These authors found that adsorption energies of glucose are higher in alkaline media compared to those in water.[23] Anota *et al.*[24] observed that the interaction between magnetic [BN-fullerene]$^{-}$ and [BN-fullerene:B6, pyramidal or triangular]$^{-}$ nanocomposites with a glucose molecule in gas and liquid media resulted in chemisorption. Another research

* Corresponding authors.
E-mail addresses: mibarod_22@hotmail.com (M. Ibarra-Rodríguez), mario.sanchez@cimav.edu.mx (M. Sánchez).

https://doi.org/10.1016/j.comptc.2023.114403
Received 26 August 2023; Received in revised form 13 November 2023; Accepted 18 November 2023
Available online 22 November 2023

focused on core–shell nanoparticles synthesized by self-assembly of a block copolymer based on phenylboronic acid poly-(*N*-isopropylacrylamide)-*block*-poly(3-acrylamidophenylboronic acid) (PNIPAM136-*b*-PAPBA16) and a fluorescent complex of glucosamine-poly (*N*-isopropylacrylamide)/Eu(III) (GA-PNIPAM)/Eu(III) that have considerable potential for applications in the delivery of glucose-sensitive drugs for diabetes treatment.[25] González Fá and coworkers [26] performed a density functional study of a glucose molecule deposited onto Pt-decorated carbon nanotubes. Their results revealed development of strong short-range bonds between oxygen atoms in β-D-glucose and platinum, characterized with adsorption energy of −1.07 eV. The interaction of glucose with H_2O and OH molecules on Pt- and Au-doped graphene surfaces was also studied, producing the binding energies for glucose-H_2O on Pt-graphene surface as high as −0.38 eV and −0.62 eV, respectively. The interaction between glucose and Pt-adorned graphene surface was stronger than that estimated for Au-adorned graphene according to the calculated reaction energy.[27] It was found that D-glucose can be adsorbed by anatase (TiO_2) surface. In this system, the presence of defects, such as surface and subsurface oxygen vacancies, causes stronger adsorption energies that favor binding of D-glucose to TiO_2 surface.[28] Following the aforementioned advances, Darwish *et al.*[29] studied interaction of a glucose molecule with hexagonal boron nitride sheets, finding that the resulting adsorption energy was about 2 eV. Recently, Yi Ma and workers used the bimetallic Ni–Co-based MOF attached to graphene oxide (GO) by a one-step hydrothermal to use it as an electrochemical enzyme-free glucose sensor.[30].

This brief literature survey clearly illustrates extreme importance and timeliness of glucose adsorption problem. Moreover, it strongly stimulates biomedical device development and other promising applications. Inspired by the outstanding properties of borophene and taking on the glucose sensing challenge, we performed a DFT study of glucose absorption on borophene [B_{36}] functionalized with different metal atoms (Li-K, Be-Ca, and Al-Ga). The full material characterization toolkit included study of molecular orbitals, calculation of chemical molecular descriptors, NBO analysis, study of theoretical infrared spectra and calculation of glucose adsorption energy in gaseous or aquatic media. We aim on production of guidelines for design and improvement of functionalized borophene for the possible glucose sensor or glucose delivery applications.

2. Computational details

All structures were optimized and characterized by calculating their vibrational modes at the same theoretical level, using the Gaussian 09 software package.[31].

The borophene and $\mathbf{[MB_{36}]^{+}}$(M = Li, Na, K), $\mathbf{[MB_{36}]^{2+}}$ (M = Be, Mg, Ca), $\mathbf{[MB_{36}]^{3+}}$ (M = B, Al, Ga) structures, were calculated with the Perdew-Burke-Ernzerhof (PBE0-D3) functional[32] and def2-TZVP basis set,[33] while the most stable configurations of **glucose-**$\mathbf{[MB_{36}]^{+}}$, $\mathbf{[MB_{36}]^{2+}}$, $\mathbf{[MB_{36}]^{3+}}$ structures were optimized with the functional PBE0-D3/def2-SVP level of theory, using the Berny algorithm with the UltraFine grid (a 999,590 grid).[34] **Glucose-**$\mathbf{[MB_{36}]^{+}}$, $\mathbf{[MB_{36}]^{2+}}$, $\mathbf{[MB_{36}]^{3+}}$ geometries corresponding to the local energy minimum were selected for the NBO analysis at the same level of theory.[35] The stabilization energy $E(2)$ was calculated using the Equation (1).

$$E(2) = \Delta Eij = qi\frac{F(i,j)^2}{j-i} \quad (1)$$

where q_i is the donor orbital occupancy; ε_i, ε_j are diagonal elements (orbital energies) and *F(i,j)* is the off-diagonal NBO Fock matrix element.

First-principles simulations are currently used to investigate the gas sensing material. [36 37 38] We have chosen the functional hybrid PBE0 because it is widely applicable and provides good results for various molecular systems containing both light and heavy atoms. The PBE0 functional features good accuracy for atomic energies, structural geometry, dissociation energies, and electronic and magnetic properties. [39 40].

The adsorption energy E_{ads} was defined as a difference

$$\Delta E_{ads} = E_{gl-MB36} - (E_{MB36} + E_{gl}) \quad (2)$$

where $E_{gl\text{-}MB36}$ is the total energy of $\mathbf{MB_{36}}$ coordinated to a glucose molecule, E_{MB36} and E_{gl} are the energies of a borophene fragment functionalized with a metal atom and a free glucose molecule, respectively. The energies of each compound were calculated for a single point using the PBE0-D3/def2-TZVP functional/basis set.

The quantum molecular descriptors used to characterize the systems include ionization potential ($I = -E_{HOMO}$), electron affinity ($A = -E_{LUMO}$), global hardness ($\eta = (I - A)/2$),[41] electronegativity ($\chi = I + A/2$), electron chemical potential ($\mu = -(I + A)/2$),[42] electrophilicity index ($\omega = -\mu^2/2\eta$)[43] and chemical softness ($S = 1/2\eta$).

3. Results and discussion

3.1. The geometry and optimization of borophene fragment

The borophene fragment optimized with PBE0-D3/def2-TZVP is not flat but rather slightly convex. It is described with the C_{6V} point group symmetry. The distance between boron atoms in the central hexagonal-shaped cavity is 3.307 Å (Fig. 1). The lengths of B-B bonds vary in the range of 1.576–1.653 Å. These values agree well with the literature data.[10,44] The highest occupied molecular orbital (HOMO) and lowest unoccupied molecular orbital (LUMO) of borophene are characterized with the energies of −6.12 and −3.96 eV, respectively, producing the HOMO-LUMO energy gap $E_g = 2.16$ eV.

3.2. Metal atom adsorption by borophene

Calculated parameters of the optimized $\mathbf{[MB_{36}]^{+}}$, $\mathbf{[MB_{36}]^{2+}}$, $\mathbf{[MB_{36}]^{3+}}$ systems are provided in Table S1. The most stable configuration adopted by $\mathbf{[MB_{36}]^{+}}$, $\mathbf{[MB_{36}]^{2+}}$, $\mathbf{[MB_{36}]^{3+}}$ represents a non-planar structure with the C_{6V} point group symmetry, which also applies to unadorned borophene fragment (Fig. 2). Metal atoms were usually coordinated to the central cavity of the fragment, featuring stronger bonds with six surrounding boron atoms. The lengths of M−B bonds for M: Li-K, Be-Ca, and B-Ga were in the range of 1.711–3.339 Å. The B-Li bond with the length of 2.380 Å agrees well with the literature.[45,46] The computed B-Ca distance for $\mathbf{[CaB_{36}]^{2+}}$ system was 2.747 Å, which is slightly larger than that observed for the α-B sheet.[47] Listing B-M bond lengths in descending order, one obtains the following sequence of metallic elements: K > Ga > Na > Ca > Mg > Li > Al > Be > B.

The natural charge was calculated for explaining the type of interaction between B_{36} and the metal atoms. The charge on M: Li-K, Be-Ca and B-Ga atoms varies in the range (+0.712)–(+1.968). The charges on boron atoms neighboring with metal inside the cavity are negative except for the case of $\mathbf{[BB_{36}]^{3+}}$. The electron density on the boron atoms reveals that they act as donors, while the metal atom behaves as an acceptor. The band gap values calculated with PBE0-D3/def2-TZVP illustrate higher reactivity for the complexes $\mathbf{[AlB_{36}]^{3+}}$ (E_g) of 0.47 eV and $\mathbf{[GaB_{36}]^{3+}}$ (E_g) of 1.09 eV in comparison to that of $\mathbf{[LiB_{36}]^{+}}$ (E_g) of 2.06 eV, $\mathbf{[NaB_{36}]^{+}}$ (E_g) of 2.06 eV, $\mathbf{[KB_{36}]^{+}}$ (E_g) of 2.07 eV, and unadorned borophene (E_g) of 2.16 eV.

Table S1 present quantum molecular descriptors for the plain B_{36} system and for metal-adorned borophene $\mathbf{[MB_{36}]^{+}}$, $\mathbf{[MB_{36}]^{2+}}$, $\mathbf{[MB_{36}]^{3+}}$. Global hardness η and electrophilicity index ω can be used for describing the degree of chemical reactivity and stability (Fig. 3).[43] The global hardness of unadorned borophene fragment is higher than that of $\mathbf{[AlB_{36}]^{3+}}$ and $\mathbf{[GaB_{36}]^{3+}}$, suggesting that Al and Ga are more reactive and less stable compared to non-modified B_{36}. Electron

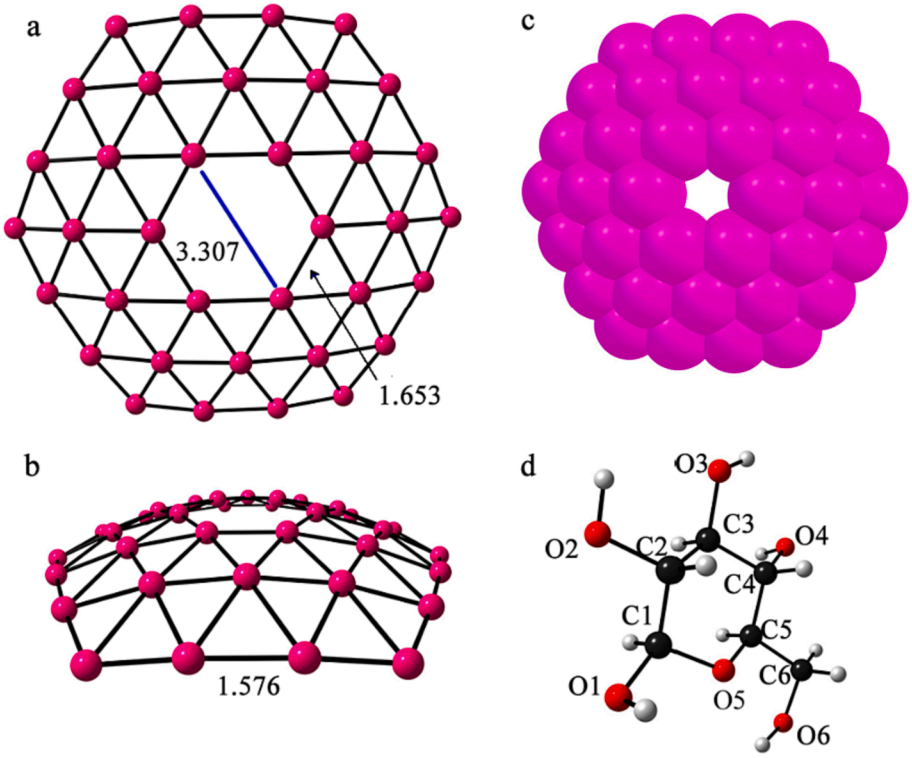

Fig. 1. Optimized borophene fragment calculated with the PBE0-D3/def2-TZVP a) top and b) side views; c) space-filling representation of the model; d) glucose molecule visualized at the same scale. The principal dimensions of the B_{36} central cavity (bonding site) are expressed in Å.

chemical potential (μ) and electrophilicity index (ω) for the plain borophene are −5.040 and −13.684 eV, respectively. The value of μ becomes strongly negative for higher oxidation degrees (Fig. 3), while the value of ω grows by about 76.8 eV, compared to non-modified borophene. High electrophilicity index displays strong capacity of $\mathbf{[MB_{36}]^{+}}$, $\mathbf{[MB_{36}]^{2+}}$, $\mathbf{[MB_{36}]^{3+}}$ systems to accept electrons. When borophene fragment absorbs M: Li-K, Be-Ca, and B-Ga, it results in less chemically-stable systems. The increase in the dipole moment for $\mathbf{[KB_{36}]^{+}}$, $\mathbf{[CaB_{36}]^{2+}}$, and $\mathbf{[GaB_{36}]^{3+}}$ in comparison to that of the plain borophene (11.311, 11.167, and 3.953 debye versus 2.600 debye) suggests an increased solubility of the resulting complex in a polar solvent (Fig. 3).

3.3. The adsorption of glucose on M-borophene

Our simulations of glucose, interacting with $\mathbf{[MB_{36}]^{+}}$, $\mathbf{[MB_{36}]^{2+}}$, $\mathbf{[MB_{36}]^{3+}}$ systems, showed that the former assumes a vertical position close to the metal atom, with which it coordinates oxygen atoms O1 and/or O2. The **glucose-**$\mathbf{[MB_{36}]^{+}}$, **glucose-**$\mathbf{[MB_{36}]^{2+}}$, **glucose-**$\mathbf{[MB_{36}]^{3+}}$ structure features C_1 point group symmetry (Fig. 4). The interaction of glucose molecule with $\mathbf{[GaB_{36}]^{3+}}$ is so strong that gallium atom is removed from borophene fragment.

Table S2 list the principal parameters of the systems studied except for the case of Ga-adorned borophene due to the afore mentioned situation. The calculated bond B-M lengths for M: Li-K, Be-Ca, and B-Ga increase upon coordination of glucose. For the case of $\mathbf{[KB_{36}]^{+}}$, this bond length increases up to 17%. The M−O distances in **glucose-**$\mathbf{[MB_{36}]^{+}}$, **glucose-**$\mathbf{[MB_{36}]^{2+}}$, **glucose-**$\mathbf{[MB_{36}]^{3+}}$ are about 1.484–2.659 Å. Sorting the M−O bond lengths in descending order, one obtains the following sequence: K-O > Ca-O > Na-O > Mg-O > Li-O > Al-O > Be-O > B-O. When compared to the isolated glucose molecule with C1-O1 bond 1.397 Å long and *C*2-O2 bond 1.427 Å long, one can observe a slight increase of the corresponding inter-atomic distances.

The observed charge on the M atoms (M: Li, Na, K, Be, Mg, Ca, B, Al) after glucose adsorption are + 0.663, +0.883, +0.883, +1.185, +1.599, +1.514, +0.705, and + 0.850, respectively. The $\mathbf{[MB_{36}]^{+}}$, $\mathbf{[MB_{36}]^{2+}}$, $\mathbf{[MB_{36}]^{3+}}$ systems in general feature mild charge decrease, except for the case of boron. Natural charge analysis reveals that glucose delocalizes charges on metal atoms, and on oxygens atoms of the coordinated molecule itself. The oxygen atoms O1 and O2 feature the most negative charge in **glucose-**$\mathbf{[MB_{36}]^{+}}$, **glucose-**$\mathbf{[MB_{36}]^{2+}}$, **glucose-**$\mathbf{[MB_{36}]^{3+}}$ systems. Due to this, they represent the best Lewis base with lone pairs, which tend to react with electron-deficient M site coordinated to the borophene fragment.

Infrared spectra of non-modified $\mathbf{B_{36}}$ and $\mathbf{[MB_{36}]^{+}}$, $\mathbf{[MB_{36}]^{2+}}$, $\mathbf{[MB_{36}]^{3+}}$ systems are shown in Fig. 6a. The vibrational modes of M−B bonds appear in the low frequency region (80–500 cm^{-1}). The main peaks corresponding to the cases of Li, Na, Mg, and Ca-adorned borophene reveal stretching vibrations of boron-metal bond with the corresponding spectral peaks located at 319, 212, 295, and 252 cm^{-1}. Upon coordination of the glucose molecule, the system becomes less ordered (Fig. 6b). The peaks of B-O stretching vibrations can be seen in the range of 150 – 800 cm^{-1}. The peak corresponding to Li is located at 494 cm^{-1}, for Na: 212 cm^{-1}, for Be: 575 cm^{-1}, for Mg: 367 cm^{-1}, for Ca: 252 cm^{-1}, for A1: 587 cm^{-1}, and for B: 782 cm^{-1}. The spectral bands corresponding to the vibrations of glucose molecule appear in the range of 3000–4000 cm^{-1}. The calculated infrared spectra offer useful data for future experimental work on borophene-based glucose sensors.

The coordination of glucose molecule with $\mathbf{[MB_{36}]^{+}}$, $\mathbf{[MB_{36}]^{2+}}$, $\mathbf{[MB_{36}]^{3+}}$ produces strong interactions characterized with adsorption energies of −34.22 to −135.24 kcal/mol. In the cases of mono-charged compounds $\mathbf{[LiB_{36}]^{+}}$, $\mathbf{[NaB_{36}]^{+}}$ and $\mathbf{[KB_{36}]^{+}}$, the energy cost of glucose adsorption is equal to −43.63, −40.83 and −34.22 kcal/mol, respectively, exceeding the values reported for single-walled carbon nanotubes with Pt (−24.68 kcal/mol),[26] Pd-doped graphene (−10.13 kcal/mol),[23] Pt-graphene (−8.76) and Au-graphene (−16.37 kcal/mol). See Table 1 [27] For compounds bearing larger charge $\mathbf{[BeB_{36}]^{+2}}$, $\mathbf{[MgB_{36}]^{+2}}$, $\mathbf{[CaB_{36}]^{+2}}$, $\mathbf{[BB_{36}]^{+3}}$, and $\mathbf{[AlB_{36}]^{+3}}$, the adsorption energy overcomes −76 kcal/mol, indicating a very good adsorption similar to that reported for Pt-decorated single-walled carbon nanotubes

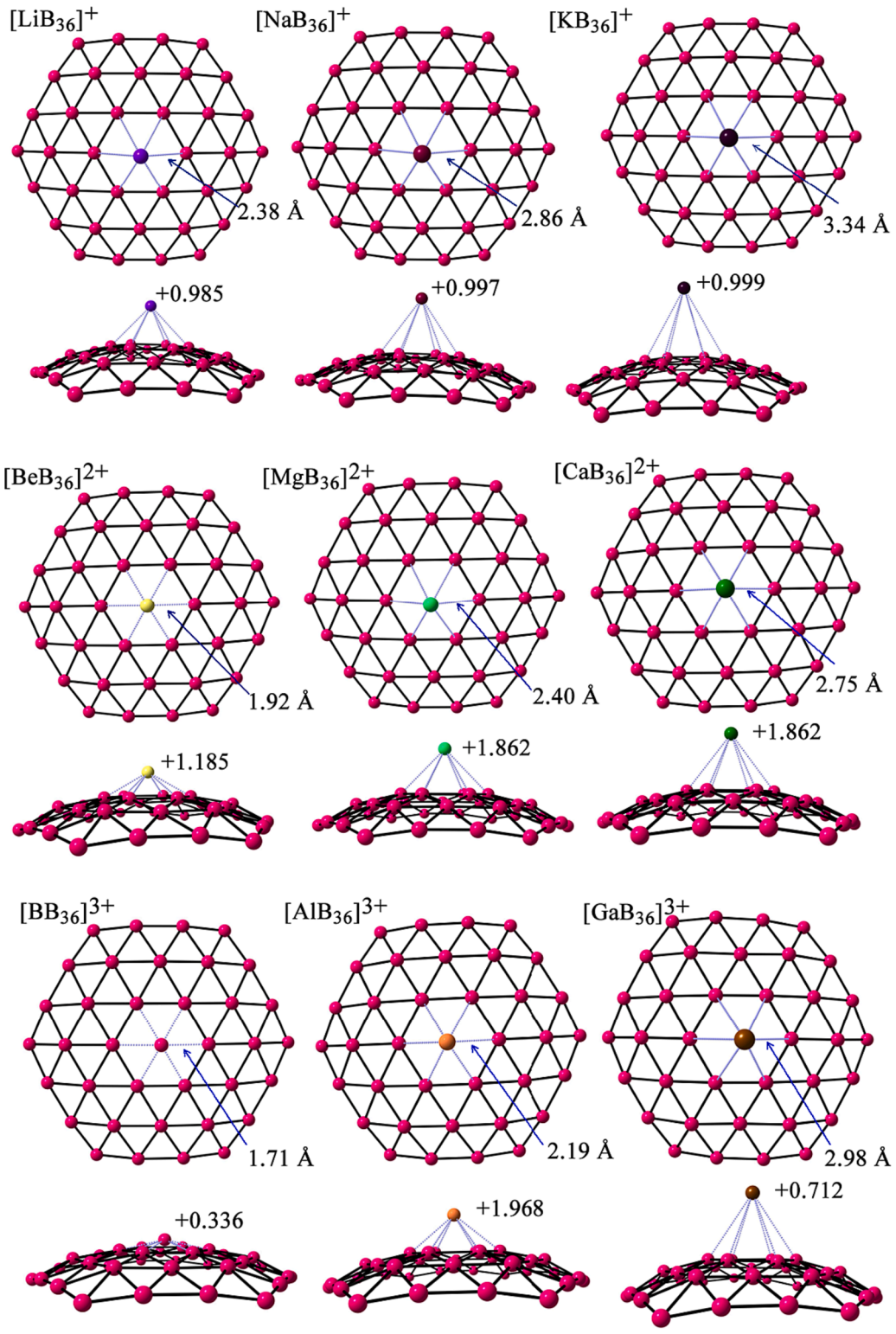

Fig. 2. Top and side views of the different $[MB_{36}]^{+}$, $[MB_{36}]^{2+}$, $[MB_{36}]^{3+}$ systems with the M−B bond lengths indicated for the central cavity. The numbers shown in the side view figures correspond to the natural charges located on the metal and boron atoms.

(−74.37 kcal/mol), which was calculated using PBE functional.[48] The adsorption energy corresponding to **glucose-**$[AlB_{36}]^{+3}$ is −135.24 kcal/mol, being more than five times larger in comparison to the interaction intensity obtained for Al-doped boron nitride (−26.29 kcal/mol).[29] Such elevated E_{ads} can be attributed to the higher positive charge predicted for the studied systems, which produces stronger interaction between glucose molecule and the coordinated metal atom. Thus, $[MB_{36}]^{+}$, $[MB_{36}]^{2+}$, $[MB_{36}]^{3+}$ structures feature excellent physisorption ease for glucose.

The energies characterizing the highest occupied molecular orbital and lowest unoccupied molecular orbital were used to calculate HOMO-LUMO gap E_g for **glucose-**$[MB_{36}]^{+}$, $[MB_{36}]^{2+}$, $[MB_{36}]^{3+}$ systems (Table S2, Fig. 5). The value of E_g increases after successful adsorption. The most pronounced variation of 357% was observed for $[AlB_{36}]^{+3}$,

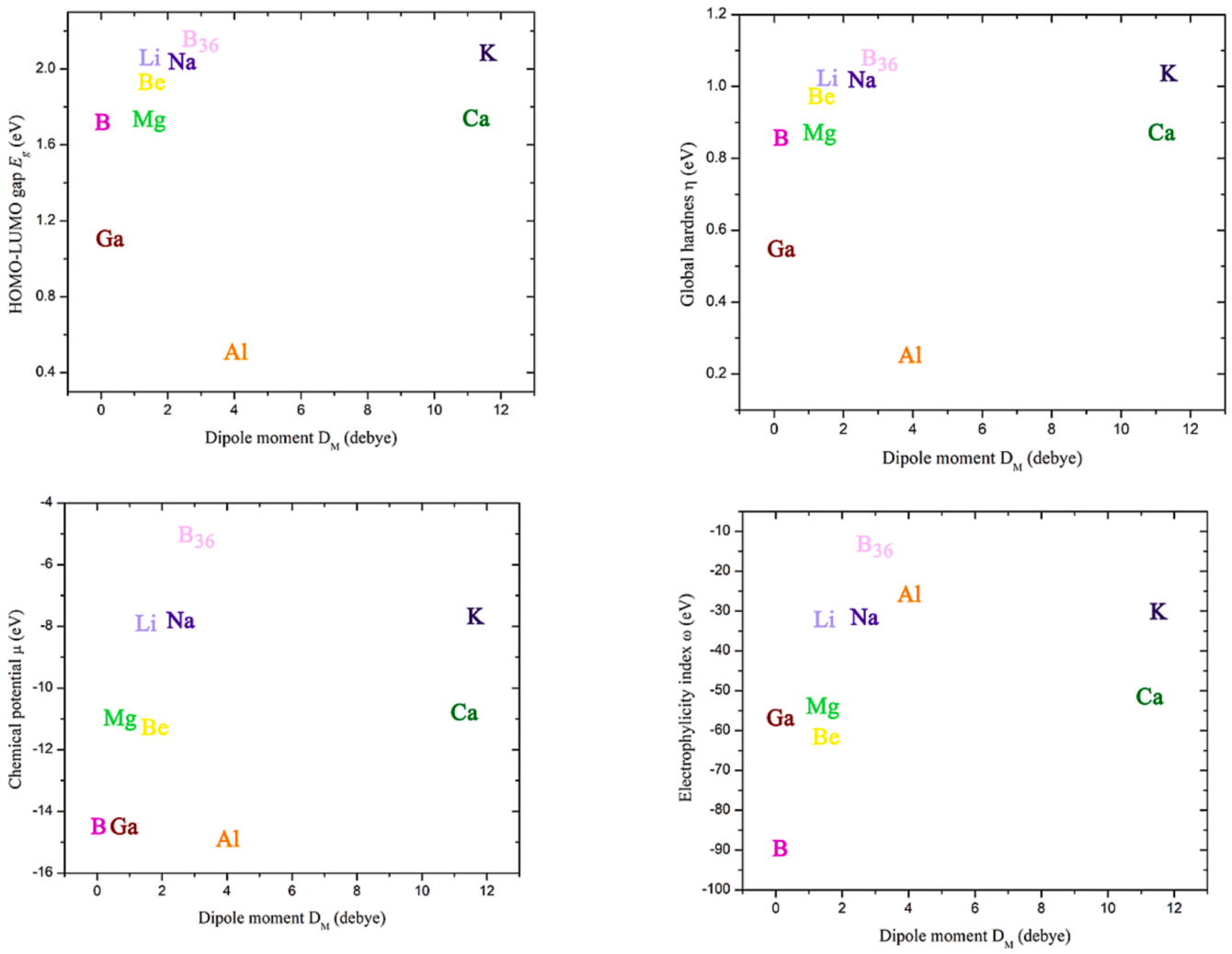

Fig. 3. Quantum molecular descriptors (HOMO-LUMO gap E_g, global hardness η, chemical potential μ, and global electrophilicity index ω vs Dipole moment Dm) for the plain borophene and $[MB_{36}]^{+}$, $[MB_{36}]^{2+}$, $[MB_{36}]^{3+}$ systems calculated with PBE0-D3/def2-TZVP method.

where the gap changed from 0.47 to 1.68 eV. Dipole moment in $[MB_{36}]^{+}$, $[MB_{36}]^{2+}$, $[MB_{36}]^{3+}$ systems are on the level of 0.235–11.311 debye. The coordination of glucose rises D_M to the levels of 5.070, 5.377, 1.871, 14.086, and 7.392 debye for $[LiB_{36}]^{+}$, $[NaB_{36}]^{+}$, $[MgB_{36}]^{2+}$, $[BB_{36}]^{3+}$, and $[AlB_{36}]^{3+}$, respectively, which indicates increasing polarization degree. Chemical potential μ, global hardness η, and electrophilicity index ω were calculated to establish the reactivity level characterizing glucose –$[MB_{36}]^{+}$, $[MB_{36}]^{2+}$, $[MB_{36}]^{3+}$ interaction (Table S2). Global hardness for all systems decreases for higher oxidation states.

Ionization potential of $[LiB_{36}]^{+}$, $[NaB_{36}]^{+}$, and $[KB_{36}]^{+}$ is lower than that of $[BeB_{36}]^{+2}$, $[MgB_{36}]^{+2}$, $[CaB_{36}]^{+2}$, $[BB_{36}]^{+3}$, and $[AlB_{36}]^{+3}$, which signifies higher stability of M: Li, Na, and K systems (employing the elements from the groups (2) and (3). Increasing oxidation state of $[MB_{36}]^{+}$, $[MB_{36}]^{2+}$, $[MB_{36}]^{3+}$ leads to higher electrophilicity, which is synonymous to stronger reactivity. Upon adsorption of the glucose molecule by $[NaB_{36}]^{+}$, $[KB_{36}]^{+}$, $[MgB_{36}]^{2+}$, $[CaB_{36}]^{2+}$, $[BB_{36}]^{3+}$, and $[AlB_{36}]^{3+}$, global hardness η increases from 1.031, 1.036, 0.873, 0.876, 0.854, and 0.235 eV to 1.047, 1.047, 0.965, 0.929, 0.950, and 0.717 eV, correspondingly. These results indicate that interaction of a molecule with $[MB_{36}]^{+}$, $[MB_{36}]^{2+}$, $[MB_{36}]^{3+}$ increases stability of the material. Adsorption process produces a slight reduction in electrophilicity ω between the $[MB_{36}]^{+}$, $[MB_{36}]^{2+}$, $[MB_{36}]^{3+}$ systems and **glucose-**$[MB_{36}]^{+}$, $[MB_{36}]^{2+}$, $[MB_{36}]^{3+}$ complex, except for the case of $[AlB_{36}]^{3+}$. The HOMO-LUMO gap for $[AlB_{36}]^{3+}$ become larger after adsorption of glucose.

The addition of the glucose molecule to the $[BB_{36}]^{3+}$ system the value of electrophilicity decreases a little, but dipole moment changes drastically increasing the solubility. For the $[LiB_{36}]^{+}$ and $[NaB_{36}]^{+}$ systems, after coordination with the glucose molecule, the solubility increases slightly while for $[KB_{36}]^{+}$ and $[CaB_{36}]^{2+}$, it decreases. The variation of the dipole moment for Ca-adorned borophene is more than two times larger than that observed for $[KB_{36}]^{2+}$. At the same time, properties of compounds formed with $[BeB_{36}]^{2+}$ and $[MgB_{36}]^{2+}$ do not change notably upon adsorption of a glucose molecule (Fig. 5).

Donor/acceptor interactions between the glucose molecule and metal atoms coordinated to the borophene fragment were analyzed with NBO technique. Fig. 7 illustrates charge transfer from glucose towards the metal atom. These results identify the oxygen atoms O1 and O6 in glucose molecule as those taking on donor function; metal atom in $[MB_{36}]^{+}$, $[MB_{36}]^{2+}$, $[MB_{36}]^{3+}$ becomes an acceptor. The $[BB_{36}]^{3+}$ systems show the larges stabilization energy *E(2)* of 78.65 kcal/mol in gaseous medium. The values of *E(2)* for all systems studied correspond to a moderate donor–acceptor interaction.

The biomedical samples frequently come in a liquid form. Therefore, it is important to address the efficiency of metal-adorned borophene adsorber in the most biologically-common liquid: the aqueous solution. We studied the behavior of dissolved **glucose-**$[MB_{36}]^{+}$, **glucose-**$[MB_{36}]^{2+}$, **glucose-**$[MB_{36}]^{3+}$ systems using the PBE0-D3/def2-TZVP method in conjunction with polarizable continuum model (PCM).[49]

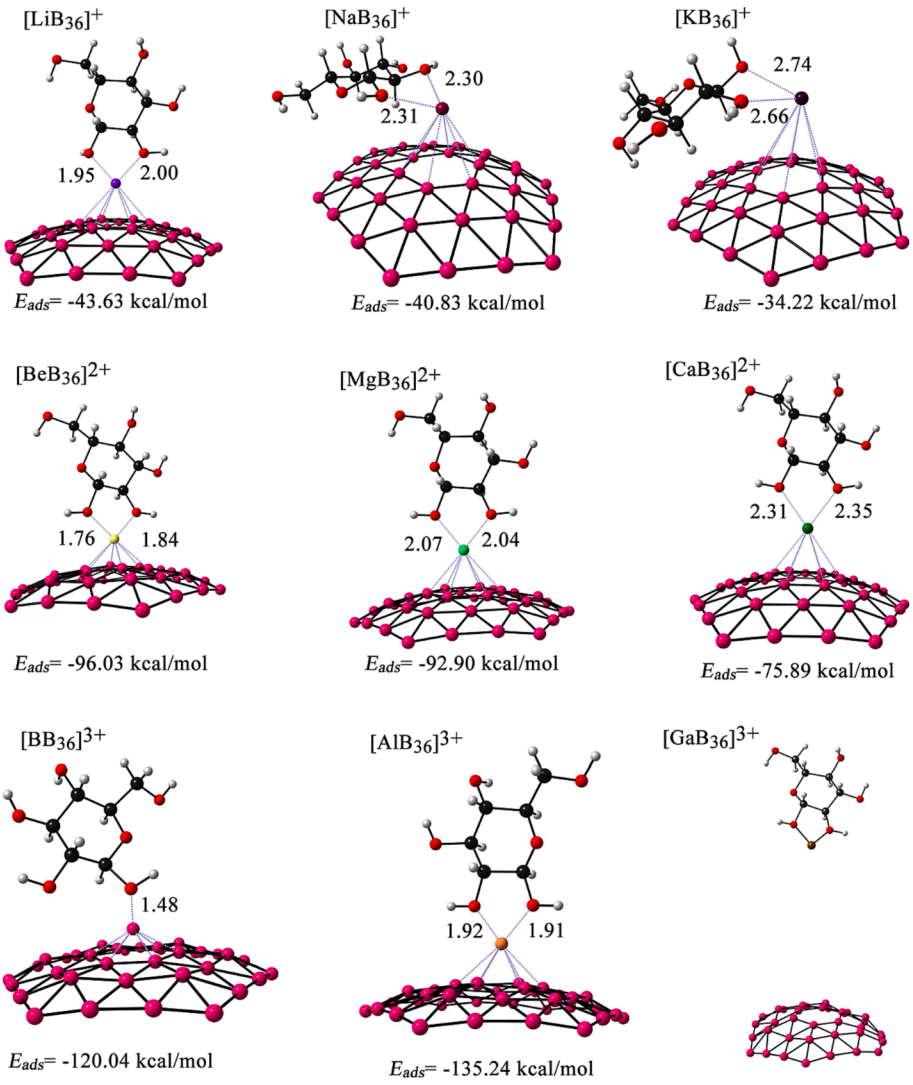

Fig. 4. Side views of **glucose-[MB$_{36}$]$^{+}$**, **glucose-[MB$_{36}$]$^{2+}$**, **glucose-[MB$_{36}$]$^{3+}$** structures. The numbers correspond to the bond length M–O (Å). Adsorption energy E_{ads} is given in kcal/mol. Individual atoms are marked with colors: pink (B), black (C), red (O), gray (H), purple (Li), light purple (Na), dark purple (K), yellow (Be), light green (Mg), green (Ca), orange (Al), and brown (Ga). (For interpretation of the references to colour in this figure legend, the reader is referred to the web version of this article.)

Table 1
Literature data on glucose adsorption energy in different systems.

System	E_{ads} (kcal/mol)	Calculation method	Ref.
[BN-Fullerene B_6]	59.04	M06	[20]
Single-walled carbon nanotubes-Pt	24.68	PBE	[21]
Pd-graphene	10.13	B3LYP/6-31 g(d,p)	[19]
Pd-*N*-graphene	14.76	B3LYP/6-31 g(d,p)	[19]
Pt-graphene	8.76	B3LYP/6-31 g(d,p)	[22]
Au-graphene	16.37	B3LYP/6-31 g(d,p)	[22]
Al-doped boron nitride	26.29	PBE	[24]
Ga-doped boron nitride	14.76	PBE	[24]
Pt single-walled carbon nanotubes	74.37	PBE	[38]
Anatase TiO_2	34.8	PBE-D3BJ	[23]
Ag_6-decorated coronene	39.9	M06-2X/LANL2DZ	[18]

The adsorption energies in water appear to be smaller than those observed under gas-phase operation (Table 2). Although adsorption energy E_{ads} for **glucose-[MB$_{36}$]$^{+}$** systems decreases from 72% to 66% when the process is carried out in water, the resulting value is still high enough. In the particular case of **glucose-[CaB$_{36}$]$^{2+}$** system, adsorption energy in water drops by 82% of the corresponding gas-phase value. In general, E_{ads} for **glucose-[MB$_{36}$]$^{+}$**, **glucose-[MB$_{36}$]$^{2+}$** systems vary between –11.5 and –55.5 kcal/mol in water, making drug release more efficient than that possible in the gaseous medium.

The recovery time τ for a sensor is an important parameter to determine if the material can be reused. For gas and water phase **[MB$_{36}$]$^{+}$**, **[MB$_{36}$]$^{2+}$**, **[MB$_{36}$]$^{3+}$** systems, the recovery time was calculated using the equation:

$$T = \upsilon^{-1} e^{-E_{ads}/KT} \quad (3)$$

where K represents the Boltzmann constant (8.62×10^{-5} eV K^{-1}), T stands for temperature of the system, and υ represents the attempt frequency. The recovery time values show that **[MB$_{36}$]$^{+}$**, **[MB$_{36}$]$^{2+}$**, **[MB$_{36}$]$^{3+}$** systems in the gas phase present high times to desorb the glucose molecule, however when the **[MB$_{36}$]$^{+}$** systems are in water it presents 9.3×10^{-5} to 1.7×10^{-4} s.

The absorption spectra for **[MB$_{36}$]$^{+}$**, **[MB$_{36}$]$^{2+}$**, **[MB$_{36}$]$^{3+}$** and **glucose-[MB$_{36}$]$^{+}$**, **glucose-[MB$_{36}$]$^{+2}$**, **glucose-[MB$_{36}$]$^{+3}$** systems in gaseous and aquatic media were calculated with PBE0-D3/def2-TZVP method augmented with PCM. As one can see from Fig. 8a, the wavelengths corresponding to absorption peaks in water follow the order

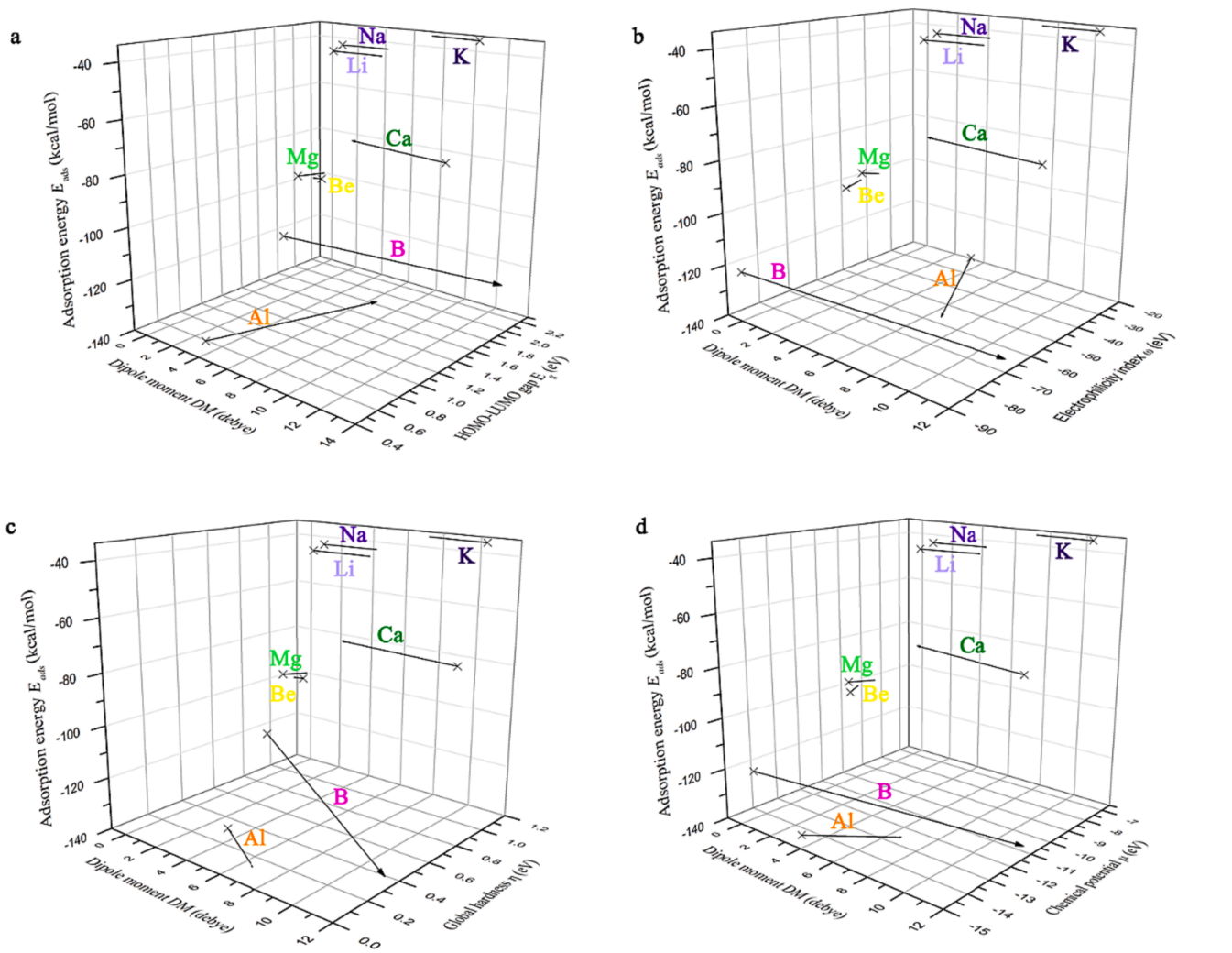

Fig. 5. Quantum molecular descriptors: **a)** HOMO-LUMO gap E_g, **b)** global electrophilicity index ω, **c)** global hardness η and **d)** chemical potential μ, for the plain $[MB_{36}]^+$, $[MB_{36}]^{2+}$, $[MB_{36}]^{3+}$ systems and **glucose-**$[MB_{36}]^+$, **glucose-**$[MB_{36}]^{2+}$, **glucose-**$[MB_{36}]^{3+}$ calculated with PBE0-D3/def2-TZVP method. The original state (×, plain $[MB_{36}]^+$, $[MB_{36}]^{2+}$, $[MB_{36}]^{3+}$) and the final state (marked with an arrow) with glucose molecule coordinated.

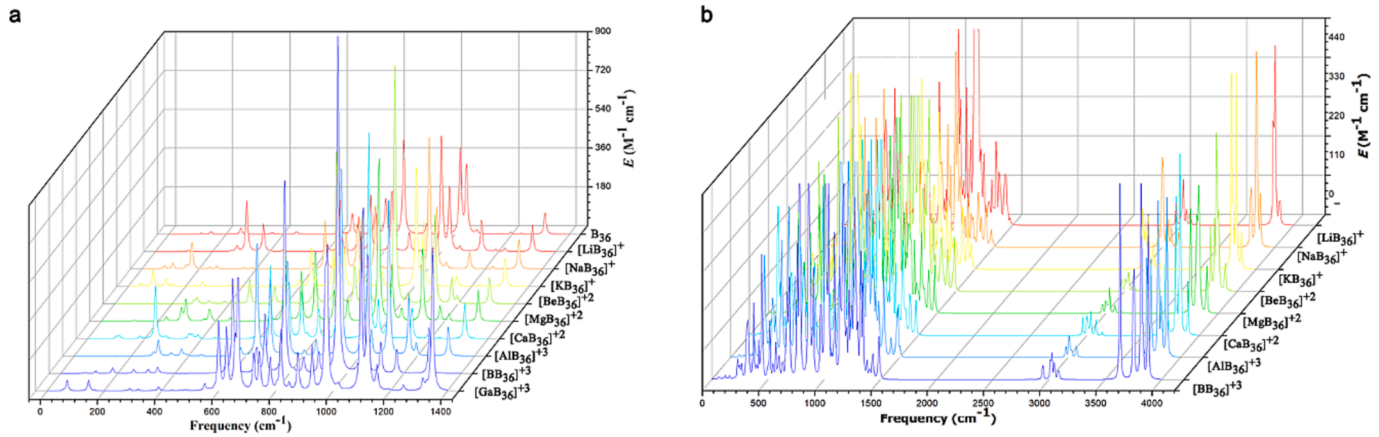

Fig. 6. Calculated IR spectra for a) $[MB_{36}]^+$, $[MB_{36}]^{2+}$, $[MB_{36}]^{3+}$ and b) **glucose-**$[MB_{36}]^+$, **glucose-**$[MB_{36}]^{2+}$, **glucose-**$[MB_{36}]^{3+}$ systems.

$[LiB_{36}]^+ > [NaB_{36}]^+ > [KB_{36}]^+$, which remains the same after adsorption of glucose. The presence of water leads to an increase of absorption wavelengths by 12 to 16 nm. The $[CaB_{36}]^{+2}$ and $[BB_{36}]^{+3}$ systems coordinated with glucose molecule show a greater displacement of 53 to 115 nm respectively (Fig. 8b,c). The coordinated glucose molecule causes a bathochromic displacement, which can be attributed to the interaction between the O—H group of glucose with the metal atom.

The results obtained in this study confirm the usefulness of $[MB_{36}]^+$, $[MB_{36}]^{2+}$, $[MB_{36}]^{3+}$ for biomedical applications centered

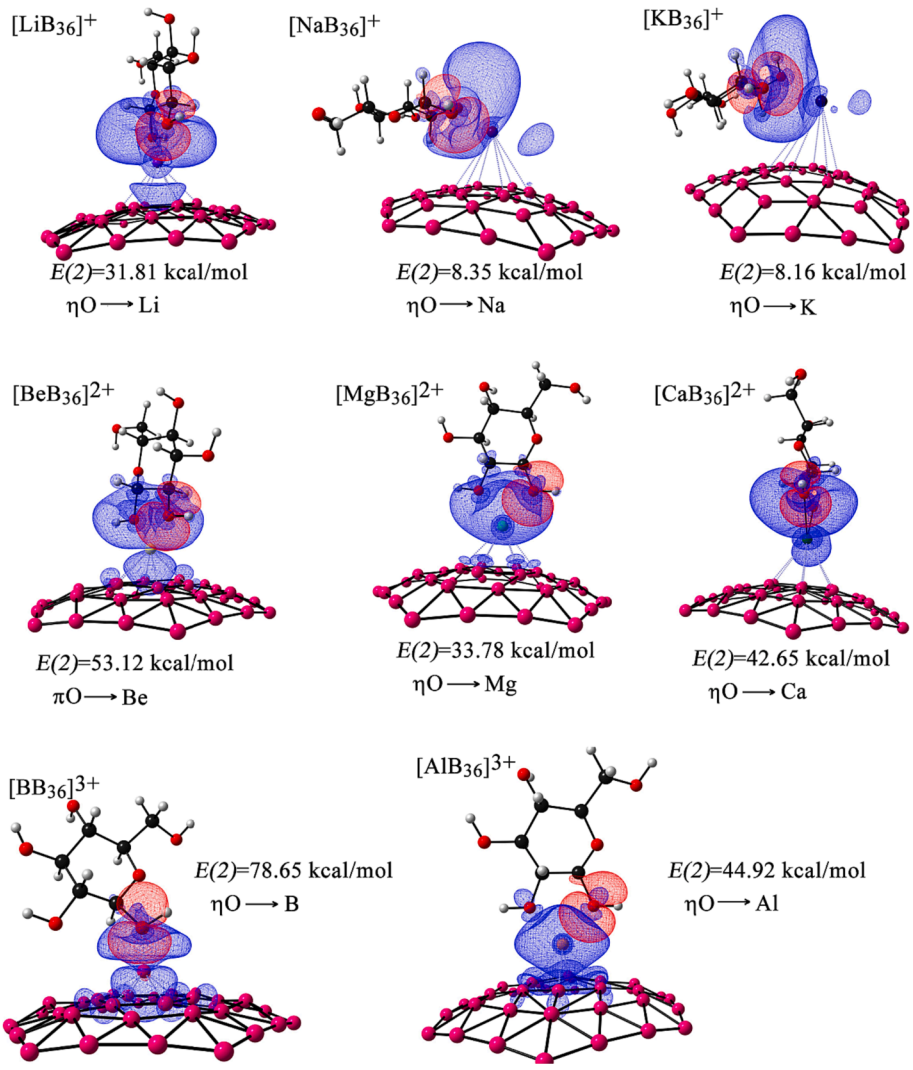

Fig. 7. NBO representation of donor and acceptor orbitals responsible for inter-molecular interactions in **glucose-[MB$_{36}$]$^{+}$**, **glucose-[MB$_{36}$]$^{2+}$**, **glucose-[MB$_{36}$]$^{3+}$** calculated with the PBE0-D3/def2-SVP method. Donor orbitals are shown in red, acceptor orbitals – in blue. *E(2)* is the energy of hyper-conjugative interaction (stabilization energy). (For interpretation of the references to colour in this figure legend, the reader is referred to the web version of this article.)

Table 2
Glucose adsorption energies for different **[MB$_{36}$]$^{+}$**, **[MB$_{36}$]$^{2+}$**, **[MB$_{36}$]$^{3+}$** systems set in gas or in water.

System	E_{ads} in gas (kcal/mol)	τ in gas (s)	E_{ads} in water (kcal/mol)	τ in water (s)
Glucose-[LiB$_{36}$]$^{+}$	−43.63	9.3×10^{18}	−12.24	9.3×10^{-5}
Glucose-[NaB$_{36}$]$^{+}$	−40.83	8.3×10^{16}	−12.61	1.7×10^{-4}
Glucose-[KB$_{36}$]$^{+}$	−34.22	1.2×10^{12}	−11.54	2.8×10^{-5}
Glucose-[BeB$_{36}$]$^{2+}$	−96.03	2.3×10^{57}	−55.53	4.9×10^{27}
Glucose-[MgB$_{36}$]$^{2+}$	−92.90	1.2×10^{55}	−26.61	3.1×10^{6}
Glucose-[CaB$_{36}$]$^{2+}$	−75.89	4.05×10^{42}	−13.79	1.3×10^{3}
Glucose-[BB$_{36}$]$^{3+}$	−120.04	9.2×10^{74}	−89.11	2.0×10^{52}
Glucose-[AlB$_{36}$]$^{3+}$	−135.24	1.3×10^{86}	−110.87	1.8×10^{68}

on glucose molecule adsorption. The systems with 1 + oxidation state, are more promising for this purpose, featuring the glucose adsorption energies from –34.22 to –43.63 kcal/mol in the gaseous medium and from –11.54 to –12.61 kcal/mol in water.

4. Conclusions

Metal-adorned borophene has a remarkable capacity for coordinating glucose, as it was shown by the analysis of several quantum molecular descriptors. All metals studied in this project (Li-K, Be-Ca, and B-Al) facilitate the adsorption of a glucose molecule. The obtained values of E_{ads} (-111 to −12 kcal/mol in water solvent) suggest glucose physisorption to **[MB$_{36}$]$^{+}$**, **[MB$_{36}$]$^{2+}$**, **[MB$_{36}$]$^{3+}$** systems. Such reduction of physisorption energy favors biological applications, including the intelligent drug delivery, because the resulting bonds with a glucose molecule in water are weaker interactions, in comparison with the gas phase adsorption. The NBO analysis identifies glucose molecule as a donor binding one or two of its oxygen atoms to a metal atom coordinated to borophene. **[MB$_{36}$]$^{+}$** systems after adsorbing the glucose molecule do not generate a change in energy gaps, moreover, the recovery time in water is very short (1.7×10^{-4} to 9.3×10^{-5} s). This result is considerably promising and stimulating for development of glucose sensors based on metal-adorned borophene. The principal

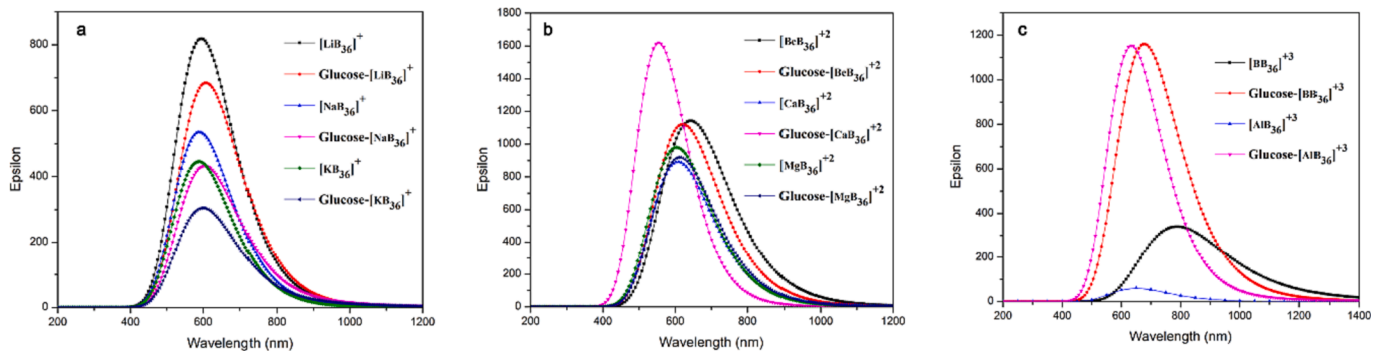

Fig. 8. Absorption spectra for systems: a) **glucose-[MB_{36}]$^{+}$**; b) **glucose-[MB_{36}]$^{+2}$**; c) **glucose-[MB_{36}]$^{+3}$** in water.

advantages of the systems studied concern the ease of structural modifications that can be used for further fine-tuning of material properties, such as degree of solubility in water.

CRediT authorship contribution statement

Marisol Ibarra-Rodríguez: Conceptualization, Methodology, Writing – original draft, Formal analysis, Validation. **Paul Horley:** Supervision, Formal analysis, Validation, Conceptualization. **Mario Sánchez:** Supervision, Project administration, Funding acquisition, Writing – review & editing.

Declaration of Competing Interest

The authors declare that they have no known competing financial interests or personal relationships that could have appeared to influence the work reported in this paper.

Data availability

No data was used for the research described in the article.

Acknowledgements

This research was financially supported by CONAHCYT of Mexico. The authors thank Rodrigo Dominguez Garcia for his highly professional support with computing resources of the supercomputer "prometeo.cim av.edu.mx".

Appendix A. Supplementary data

Supplementary data to this article can be found online at https://doi.org/10.1016/j.comptc.2023.114403.

References

[1] A. Lherbier, A.R. Botello-Méndez, J.C. Charlier, Electronic and optical properties of pristine and oxidized borophene, 2D Mater. 3 (2016), 045006.
[2] J.E. Padilha, R.H. Miwa, A. Fazzio, Directional dependence of the electronic and transport properties of 2D borophene and borophane, Phys. Chem. Chem. Phys. 18 (2016) 25491–25496.
[3] B. Mortazavi, O. Rahaman, A. Dianat, T. Rabczuk, Mechanical responses of borophene sheets: a first-principles study, Phys. Chem. Chem. Phys. 18 (2016) 27405–27413.
[4] H. Wang, Q. Li, Y. Gao, F. Miao, X.F. Zhou, X.G. Wan, Strain effects on borophene: ideal strength, negative Possion's ratio and phonon instability, New J. Phys. 18 (2016), 073016.
[5] A.P. Sergeeva, I.A. Popov, Z.A. Piazza, W.-L. Li, C. Romanescu, L.-S. Wang, A. I. Boldyrev, Understanding boron through size-selected clusters: structure, chemical bonding, and fluxionality, Acc. Chem. Res. 47 (2014) 1349–1358.
[6] B. Feng, J. Zhang, Q. Zhong, W. Li, S. Li, H. Li, P. Cheng, S. Meng, L. Chen, K. Wu, Experimental realization of two-dimensional boron sheets, Nat. Chem. 8 (2016) 563–568.
[7] Y. Valadbeigi, H. Farrokhpour, M. Tabrizchi, Adsorption of small gas molecules on B_{36} nanocluster, J. Chem. Sci. 127 (2015) 2029–2038.
[8] L. Chun-Sheng, W. Xiangfu, Y. Xiao-Juan, Y. Xiaohong, Z. Zhi, Curvature and ionization-induced reversible hydrogen storage in metalized hexagonal B_{36}, Chem. Phys. 141 (2014), 194306.
[9] A.J. Mannix, Z. Zhang, N.P. Guisinger, B.I. Yakobson, M.C. Hersam, Borophene as a prototype for synthetic 2D materials development, Nature Nanotech. 13 (2018) 444–450.
[10] E. Vessally, S.A. Javarsineh, A. Bekhradnia, A. Hosseinian, S. Ahmadi, Computational study of a B_{36} borophene as an electronic sensor for the anti-cancer drug cisplatinum, J. Comput. Electron. 20 (2021) 635–642.
[11] A. Shahbazi Kootenaei, G. Ansari, B_{36} borophene as an electronic sensor for formaldehyde: quantum chemical analysis, Phys. Lett. 380 (2016) 2664–2668.
[12] C. Xiao, K. Ma, G. Cai, X. Zhang, E. Vessally, Borophene as an electronic sensor for metronidazole drug: A computational study, J. Mol. Graph. Model. 96 (2020), 107539.
[13] S. Yadav, M.A. Sadique, A. Kaushik, P. Ranjan, R. Khan, A.K. Srivastava, Borophene as an emerging 2D flatland for biomedical applications: current challenges and future prospects, J. Mater. Chem. B 10 (2022) 1146–1175.
[14] Y. Tian, Z. Guo, T. Zhang, H. Lin, Z. Li, J. Chen, S. Deng, F. Liu, Inorganic boron-based nanostructures: synthesis, optoelectronic properties, and prospective applications, Nanomater. 9 (2019) 538.
[15] A. Omidvar, Borophene: A novel boron sheet with a hexagonal vacancy offering high sensitivity for hydrogen cyanide detection, Comput. Theor. Chem. 1115 (2017) 179–184.
[16] A. Rastgou, H. Soleymanabadi, A. Bodaghi, DNA sequencing by borophene nanosheet via an electronic response: A theoretical study, Microelectron. Eng. 169 (2017) 9–15.
[17] E. Czarniewska, K. Sielicki, K. Maślana, E. Mijowska, In vivo study on borophene nanoflakes interaction with Tenebrio molitor beetle: viability of hemocytes and short-term immunity effect, Sci. Rep. 13 (2023) 11823.
[18] M. Han, L. Zhu, J. Mo, W. Wei, B. Yuan, J. Zhao, C. Cao, Protein corona and immune responses of borophene: A comparison of nanosheet–plasma interface with graphene and phosphorene, ACS Appl. Bio Mater. 3 (2020) 4220–4229.
[19] Z. Xie, X. Meng, X. Li, W. Liang, W. Huang, K. Chen, J. Chen, C. Xing, M. Qiu, B. Zhang, G. Nie, N. Xie, X. Yan, H. Zhang, Two-dimensional borophene: properties, fabrication, and promising applications, Research 2020 (2020) 2624617.
[20] C. Huang, A. Murat, V. Babar, E. Montes, U. Schwingenschlögl, Adsorption of the gas molecules NH_3, NO, NO_2, and CO on borophene, J. Phys. Chem. 122 (2018) 14665–14670.
[21] V. Shukla, J. Wärnå, N.K. Jena, A. Grigoriev, R. Ahuja, Toward the realization of 2D borophene based gas sensor, J. Phys. Chem. C 121 (2017) 26869–26876.
[22] T. Jadoon, T. Mahmood, K. Ayub, Silver cluster (Ag6) decorated coronene as non-enzymatic sensor for glucose and H2O2, J. Mol. Graph. Model. 103 (2021), 107824.
[23] A. Caglar, D. Düzenli, I. Onal, I. Tezsevin, O. Sahin, H. Kivrak, A novel experimental and density functional theory study on palladium and nitrogen doped few layer graphene surface towards glucose adsorption and electrooxidation, J. Phys. Chem. Solids 150 (2021), 109684.
[24] E.C. Anota, M.S. Villanueva, E. Shakerzadeh, M. Castro, Adsorption and possible dissociation of glucose by the [BN fullerene-B6]− magnetic nanocomposite, In silico studies, Appl. Nanosci. 8 (2018) 455–465.
[25] G. Cui, K. Zhao, K. You, Z. Gao, T. Kakuchi, B. Feng, Q. Duan, Synthesis and characterization of phenylboronic acid-containing polymer for glucose-triggered drug delivery+, Sci Technol Adv Mate. 21 (2020) 1–10.
[26] A.J. González Fá, V. Orazi, E.A. González, A. Juan, I. López-Corral, DFT study of β-d-glucose adsorption on single-walled carbon nanotubes decorated with platinum. A bonding analysis, Appl. Surf. Sci. 423 (2017) 542–548.
[27] A. Caglar, D. Düzenli, I. Onal, I. Tezsevin, O. Sahin, H. Kivrak, A comparative experimental and density functional study of glucose adsorption and electrooxidation on the Au-graphene and Pt-graphene electrodes, Int. J. Hydrog. Energy. 45 (2020) 490–500.
[28] V. Butera, A. Massaro, A.B. Muñoz-García, M. Pavone, H. Detz, d-glucose adsorption on the TiO2 anatase (100) surface: a direct comparison between cluster-based and periodic approaches, Front. Chem. 9 (2021), 716329.

[29] A.A. Darwish, M.M. Fadlallah, A. Badawi, A.A. Maarouf, Adsorption of sugars on Al- and Ga-doped boron nitride surfaces: a computational study, Appl. Surf. Sci. 377 (2016) 9–16.
[30] Y. Ma, Y. Leng, D. Huo, D. Zhao, J. Zheng, H. Yang, P. Zhao, F. Li, C. Hou, A sensitive enzyme-free electrochemical sensor based on a rod-shaped bimetallic MOF anchored on graphene oxide nanosheets for determination of glucose in huangshui, Anal. Methods 15 (2023) 2417–2426.
[31] R. Krishnan, J.S. Binkley, R. Seeger, J.A. Pople, Self-consistent molecular orbital methods. XX. A basis set for correlated wave functions, J. Phys. Chem. 72 (1980) 650–654.
[32] J.P. Perdew, K. Burke, M. Ernzerhof, Generalized gradient approximation made simple, Phys. Rev. Lett. 77 (1997) 3865–3868.
[33] B.P. Pritchard, D. Altarawy, B. Didier, T.D. Gibson, T.L. Windus, New basis set exchange: an open, up-to-date resource for the molecular sciences community, J. Chem. Inf. Model. 59 (2019) 4814–4820.
[34] S. Grimme, J. Antony, S. Ehrlich, H. Krieg, A consistent and accurate ab initio parametrization of density functional dispersion correction (DFT-D) for the 94 elements H-Pu, J. Chem. Phys. 132 (2010), 154104.
[35] E.D. Glendening, C.R. Landis, F. Weinhold, NBO 6.0: Natural bond orbital analysis program, J. Comp. Chem. 34 (2013) 1429–1437.
[36] S. Zhai, X. Jiang, D. Wu, L. Chen, Y. Su, H. Cui, F. Wu, Single Rh atom decorated pristine and S-defected PdS_2 monolayer for sensing thermal runaway gases in a lithium-ion battery: A first-principles study, Surf. Interfaces 37 (2023), 102735.
[37] H. Wu, Y. Xia, C. Zhang, S. Xie, S. Wu, H. Cui, Adsorptions of $C_5F_{10}O$ decomposed compounds on the Cu-decorated NiS_2 monolayer: a first-principles theory, Mol. Phys. 121 (2023) e2163715.
[38] H. Cui, C. Yan, P. Jia, W. Cao, Adsorption and sensing behaviors of SF_6 decomposed species on Ni-doped C_3N monolayer: A first-principles study, Appl. Surf. Sci. 512 (2020), 145759.
[39] J. Luo, Z.Q. Xue, W.M. Liu, J.L. Wu, Z.Q. Yang, Koopmans' Theorem for Large Molecular Systems within Density Functional Theory, J. Phys. Chem. A 110 (2006) 12005–12009.
[40] A. Hicken, A.J.P. White, M.R. Crimmin, Reversible Coordination of Boron–, Aluminum–, Zinc–, Magnesium–, and Calcium-Hydrogen Bonds to Bent CuL2 Fragments: Heavy σ Complexes of the Lightest Coinage Metal, Inorg. Chem. 56 (2017) 8669–8682.
[41] R.G. Parr, R.G. Pearson, Absolute hardness: companion parameter to absolute electronegativity, J. Am. Chem. Soc. 105 (1983) 7512–7516.
[42] R.G. Parr, R.A. Donnelly, M. Levy, W.E. Palke, Electronegativity: The density functional viewpoint, J. Chem. Phys. 68 (1978) 3801–3807.
[43] R.G. Parr, L.V. Szentpály, S. Liu, Electrophilicity Index, J. Am. Chem. Soc. 121 (1999) 1922–1924.
[44] Z.A. Piazza, H.-S. Hu, W.-L. Li, Y.-F. Zhao, J. Li, L.-S. Wang, Planar hexagonal B_{36} as a potential basis for extended single-atom layer boron sheets, Nat Commun. 5 (2014) 3113.
[45] T. Liu, Y. Chen, H. Wang, M. Zhang, L. Yuan, C. Zhang, Li-decorated β_{12}-borophene as potential candidates for hydrogen storage: A first-principle study, Materials (Basel) 10 (2017) 1399.
[46] A. Lebon, R.H. Aguilera-del-Toro, L.J. Gallego, A. Vega, Li-decorated Pmmn8 phase of borophene for hydrogen storage. A van der Waals corrected density-functional theory study, Int. J. Hydrog. Energy. 44 (2019) 1021–1033.
[47] J. Wang, Y. Du, L. Sun, Ca-decorated novel boron sheet: a potential hydrogen storage medium, Int. J. Hydrog. Energy. 41 (2016) 5276–5283.
[48] M.D. Ganji, F.S. Emami Skardi, Adsorption of glucose molecule onto platinum-decorated single-walled carbon nanotubes: a dispersion-corrected DFT simulation, Fuller. Nanotub. Carbon Nanostructures 23 (2015) 273–282.
[49] S. Miertuš, E. Scrocco, J. Tomasi, Electrostatic interaction of a solute with a continuum. A direct utilizaion of AB initio molecular potentials for the prevision of solvent effects, Chem. Phys. 55 (1981) 117–129.